ARCHIVES OF ELECTRICAL ENGINEERING VOL. 65(1), pp. 141-150 (2016)

DOI 10.1515/aee-2016-0011

Magnetoacoustic tomography with magnetic induction for biological tissue imaging: numerical modelling and simulations

ADAM RYSZARD ŻYWICA

West Pomeranian University of Technology, Szczecin
Department of Electrical and Computer Engineering
Sikorskiego 37, 70-313 Szczecin, Poland
e-mail: Adam.Zywica@zut.edu.pl

(Received: 12.08.2015, revised: 12.01.2015)

Abstract: Many imaging techniques are playing an increasingly significant role in clinical diagnosis. In the last years especially noninvasive electrical conductivity imaging methods have been investigated. Magnetoacoustic tomography with magnetic induction (MAT-MI) combines favourable contrast of electromagnetic tomography with good spatial resolution of sonography. In this paper a finite element model of MAT-MI forward problem has been presented. The reconstruction of the Lorentz force distribution has been performed with the help of a time reversal algorithm.

Key words: finite element analysis, magnetoacoustic effects, medical diagnostic imaging, reconstruction algorithms

1. Introduction

Many various imaging techniques are playing an increasingly significant role in biomedical research and clinical diagnosis. In recent years noninvasive electrical conductivity imaging has been especially investigated, because electrical properties of biological tissues are known to be sensitive to physiological and pathological conditions of living organisms. For instance, human breast cancer or liver tumor cells have a significantly higher electrical conductivity than a healthy tissue [1, 2].

During the past several decades a lot of noninvasive imaging methods have been developed and utilized in order to reconstruct the electrical conductivity distribution of biological tissues, e.g.: electrical impedance tomography (EIT), magnetic induction tomography (MIT), magnetic resonance electrical impedance tomography (MREIT), magnetoacoustic tomography (MAT) [3].

Recently, a new technique of bio-impedance tomography, i.e. magnetoacoustic tomography with magnetic induction (MAT-MI) was developed by coupling two fundamental physical

phenomena, namely: ultrasound and magnetism. Such a combination eliminates the shielding effect and low spatial resolution of previous imaging modalities. The simulation process of MAT-MI involves two main parts. At first, the so-called *forward problem* is formulated, which aim is to express the acoustic pressure induced in a biological tissue. Then, the second part, called the *inverse problem*, takes places. It consists of two steps: reconstructing the distribution of Lorentz force divergence according to acoustic signals collected by sensors and finally reconstructing the distribution of electrical conductivity [3-6].

In this paper a finite element model of the MAT-MI forward problem has been presented. According to the inverse problem, the first step has been performed (i.e. a reconstruction of Lorentz force distribution), and for conductivity distribution theoretical considerations along with governing equations have been provided. The Lorentz force divergence reconstruction has been achieved with the help of a freely available toolbox in the Matlab environment, called k-Wave, which is based on a time reversal image reconstruction algorithm. It has been demonstrated that the MAT-MI simulation allows for detection and reconstruction of the boundaries between regions of different electrical conductivities.

2. Fundamentals of MAT-MI theory

Let us assume that an object (inner layer shown in Fig. 1) of higher conductivity equal to σ_1 (muscle or brain tissue equivalent) and an arbitrary shape is placed in a medium (outer layer) of lower conductivity σ_0 (skull or fat equivalent). If the currents are injected (like in EIT or MAT), the outer layer will significantly reduce the amount of current flowing into the object. As a consequence, the overall tomography system sensitivity to the changes of the object's conductivity will be decreased. Such a phenomenon is commonly called the *shielding effect* [7]. In order to avoid this problem magnetic induction tomography MIT has been developed, where the eddy currents are generated in the object due to the use of magnetic induction [8]. However, according to this imaging method no high spatial resolution has been reported. Additionally, the inverse problem in the MIT and EIT approaches is ill-posed which affects possible solutions. In order to avoid this shielding effect and achieve high spatial resolution magnetoacoustic tomography with magnetic induction (MAT-MI) has been proposed. This method is relatively new imaging modality which combines favourable contrast of electromagnetic tomography with good spatial resolution of sonography. In MAT-MI an object to be imaged is placed in static and time-varying (pulsed) external magnetic fields. The time-varying magnetic field induces eddy currents in the object's volume even, if the outer layer is insulating ($\sigma_0 = 0$). Accordingly, the Lorentz force (result of interaction between a static magnetic field and eddy currents) is generated in the object and finally acoustic vibrations are emitted. Propagated acoustic waves can be acquired by a set of piezoelectric transducers located around the object. Collected signals are then used for electrical conductivity image reconstruction, which leads to well-posed imaging inverse problem [7]. The illustration of the MAT-MI concept has been shown in Figure 1.

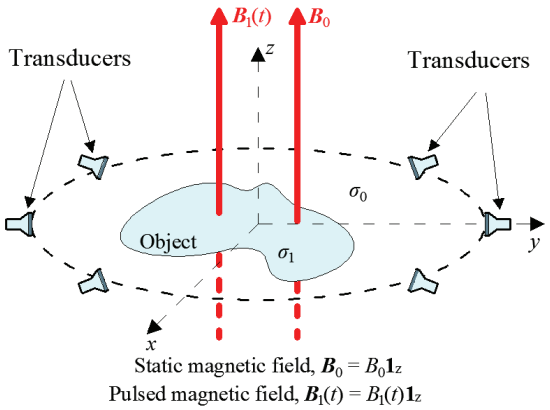

Fig. 1. Illustration of MAT-MI concept

2.1. Forward problem formulation

Taking into account the Cartesian coordinate system (x, y, z) it is assumed that the object to be imaged is homogeneous in the direction of the z-axis. The static $\mathbf{B}_0(\mathbf{r})$ ($\mathbf{r}$ is the position vector) and pulsed $\mathbf{B}_1(\mathbf{r}, t)$ magnetic fields are uniform and also in that direction. In this case, the resultant induced eddy currents density vector $\mathbf{J}(\mathbf{r}, t)$ is limited in the xy plane. Therefore, in general the 3D MAT-MI forward model can be simplified as a two-dimensional thin slab with nonuniform conductivity distribution $\sigma(\mathbf{r})$ placed in the xy ($z = 0$) plane for a given magnetic excitation. Schematic diagram of 2D planar plane MAT-MI model is shown in Figure 2.

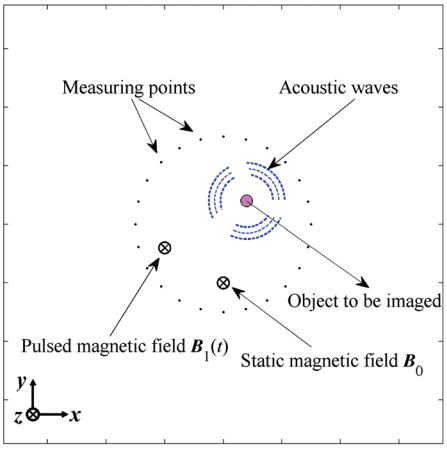

Fig. 2. Schematic diagram of 2D MAT-MI model

The magnetic stimulation $\mathbf{B}_1(\mathbf{r}, t)$ can be represented by the curl of its magnetic vector potential $\mathbf{A}(\mathbf{r}, t)$: $\mathbf{B}(\mathbf{r}, t) = \nabla \times \mathbf{A}(\mathbf{r}, \mathrm{t})$. The conductivity values are small enough that we can ignore the effect of secondary magnetic field $\mathbf{A}(\mathbf{r}, t) \approx \mathbf{A}_p(\mathbf{r}, \mathrm{t})$, where $\mathbf{A}_p(\mathbf{r}, t)$ denotes the

primary vector potential produced by stimulating coil in absence of the object. Additionally, in MAT-MI for driving the stimulating coil μs level current pulses are used and hence the magnetic induction problem can be considered as quasi-static. The electric field inside the object and the eddy currents density can be expressed as [8]:

$$\mathbf{E}(\mathbf{r},t) = -\frac{\partial \mathbf{A}(\mathbf{r},t)}{\partial t} - \nabla\Phi(\mathbf{r},t)\ ,\ \mathbf{J}(\mathbf{r},t) = \sigma(\mathbf{r})\mathbf{E}(\mathbf{r},t), \tag{1}$$

where: $\Phi(\mathbf{r}, t)$ – electric scalar potential.

The calculation of the unknown magnetic vector and electric scalar potentials in (1) have been described in details in previous papers [8]. Assuming that the magnetic field stimulation pulse is short enough, after separating the spatial and temporal functions of the time-varying magnetic fields, the Lorentz force density acting on eddy currents over unit volume can be written as [4, 7, 8]:

$$\mathbf{F}(\mathbf{r},t) = [\mathbf{J}(\mathbf{r}) \times \mathbf{B}_0(\mathbf{r})]\delta(t), \tag{2}$$

where: $\delta(t)$ is the Dirac delta function (delta function) in time domain.

The force resulting from Equation (2) leads to mechanical vibrations and generates an acoustic wave governed by the following wave Equation [7, 9]:

$$\nabla^2 p(\mathbf{r},t) - \frac{1}{c_s^2}\frac{\partial^2 p(\mathbf{r},t)}{\partial t^2} = \nabla \cdot [\mathbf{J}(\mathbf{r}) \times \mathbf{B}_0(\mathbf{r})]\delta(t), \tag{3}$$

where: $p(\mathbf{r}, t)$ is the acoustic pressure at spatial point $\mathbf{r}$, $c_s = (\rho_0 \cdot \beta_s)^{-1/2}$ is the acoustic speed, ρ_0 is the density of the object at rest and β_s is the adiabatic compressibility of the medium. It should be noted, that in this case $\mathbf{J}(\mathbf{r})$ has the unit of $A \cdot s/m^2$ and based on this assumption the next equations are constructed [7].

By using Green's function, the Equation (3) can be solved as [7, 8]:

$$p(\mathbf{r},t) = -\frac{1}{4\pi}\int_V \nabla_{\mathbf{r}'} \cdot [\mathbf{J}(\mathbf{r}') \times \mathbf{B}_0(\mathbf{r}')]\frac{\delta\left(t - \dfrac{R}{c_s}\right)}{R}\,\mathrm{d}\mathbf{r}', \tag{4}$$

where: $R = |\mathbf{r} - \mathbf{r}'|$, and the integration is over the sample volume containing the acoustic source.

2.2. Inverse problem formulation

In the inverse problem the acoustic pressure signals around the object, either measured or simulated, are used for reconstruction of the conductivity distribution $\sigma(\mathbf{r})$ within the object. Generally, the inverse problem can be divided into two steps. First, the source term $\nabla \cdot (\mathbf{J} \times \mathbf{B}_0)$ of the wave equation can be reconstructed using time reversal technique. The main idea of the time reversal method is that the acoustic wave propagation can be reversed in time and played back. The method can be applied to every phenomenon described by the so called time-reversal-invariant equations (which contain only derivatives of an even order). The time reversal technique usually consists of two parts. At first an acoustic pressure $p(\mathbf{r}, t)$ is generated

by a source (in experiments or in simulations). This acoustic pressure is either measured by transducers located circumferentially (as shown in Fig. 1) or calculated at 'measuring points' (as shown in Fig. 2) as a function of time and stored. If all the recorded signals are reversed in time and reemitted from the position where they have been recorded, the resulting vibration will converge back to the point where it was originally emitted. The duration of this recording is given by T. Next, the measurements at each position are reversed in time, which results in the time reversed signals [10, 11]:

$$p_{TR}(\mathbf{r},t) = p(\mathbf{r},T-t), \tag{5}$$

In the second step, the measuring points are used as sources where the time reversed signals p_{TR} are applied simultaneously. The resulting waves propagate back through the medium and interfere constructively at the position of the original source.

Using the time reversal method, the acoustic source can be described as follows [5, 7]:

$$\nabla\cdot[\mathbf{J}(\mathbf{r})\times\mathbf{B}_0(\mathbf{r})] \approx -\frac{1}{2\pi c_S^3}\int_{S_d}\frac{\mathbf{n}\cdot(\mathbf{r}-\mathbf{r}_d)}{|\mathbf{r}-\mathbf{r}_d|^2}\left.\frac{\partial^2 p(\mathbf{r}_d,t)}{\partial t^2}\right|_{t=|\mathbf{r}-\mathbf{r}_d|/c_S} dS_d, \tag{6}$$

where: $\boldsymbol{r}_d$ is the detection point on the surface S_d and $\mathbf{n}$ is a unit vector normal to the surface S_d at $\boldsymbol{r}_d$.

In the second step, the conductivity distribution $\sigma(\mathbf{r})$ is reconstructed from $\nabla\cdot[\mathbf{J}(\mathbf{r}) \times \mathbf{B}_0(\mathbf{r})]$, however, it is not an easy task. In order to overcome this problem two methods have been proposed [7]. In the first method, called *piecewise distribution*, there is no need to change the direction of the static magnetic field $\mathbf{B}_0$. Under assumption that the object to be imaged is piecewise smooth the following approximate formula can be derived [7, 8]:

$$\sigma(\mathbf{r}) \approx \frac{\nabla\cdot[\mathbf{J}(\mathbf{r})\times\mathbf{B}_0(\mathbf{r})]}{\mathbf{B}_1(\mathbf{r})\cdot\mathbf{B}_0(\mathbf{r})}, \tag{7}$$

Equation (7) does not hold on the boundary between region with different conductivity, therefore final iterative algorithm has to be applied [7]:

$$\sigma_n(\mathbf{r}) \approx \frac{-[\nabla\times\mathbf{J}(\mathbf{r})]\cdot\mathbf{B}_0(\mathbf{r})}{[\mathbf{B}_1(\mathbf{r})+\nabla(1/\sigma_{n-1})\times\mathbf{J}_{n-1}]\cdot\mathbf{B}_0}, \tag{8}$$

The second method requires to change direction of the static magnetic field $\mathbf{B}_0$ (more than one set of measurements or calculations is needed). In quasi-static case the continuity equation takes the following form [7, 8]:

$$\nabla\cdot\mathbf{J}(\mathbf{r}) = 0. \tag{9}$$

The term $\mathbf{B}_0(\mathbf{r})\cdot(\nabla \times \mathbf{J}(\mathbf{r}))$ can be reconstructed from the pressure calculated around the object. In the case of making three sets of calculations, where $\mathbf{B}_0(\mathbf{r})$ is directed along three perpendicular directions, the term $\nabla \times \mathbf{J}(\mathbf{r})$ can be determined. Finally the conductivity can be reconstructed from the following Equation [7]:

$$\sigma(\mathbf{r}) = \frac{-[\nabla\times\mathbf{J}(\mathbf{r})]\cdot\mathbf{J}(\mathbf{r})}{\mathbf{B}_1(\mathbf{r})\cdot\mathbf{J}(\mathbf{r})}. \tag{10}$$

3. Numerical results

The MAT-MI forward problem simulations have been performed with Comsol Multi-physics software, which is based on the finite element method (FEM). In order to solve this problem 10 finite elements per acoustic wavelength have been applied. It is consistent with the wave theory and allows for achieving reasonable accuracy.

The 2D planar quasi static study has been chosen. The first analysed model geometry, shown in Figure 2, consists of two layers placed non-concentrically with conductivities: outer layer with $\sigma_0 = 0$ (distilled water equivalent), inner layer (i.e. object to be imaged) with exemplary conductivity $\sigma_1 = 10$ S/m and diameter equal to 4 mm. It is assumed that the inner and outer layer are acoustically homogeneous without any reflections, dispersion and attenuation. The acoustic velocity c_s was set to 1490 m/s. The uniform magnetic flux density $\mathbf{B}_0$ value has been set to 1 T. In case of pulsed uniform magnetic field $\mathbf{B}_1(t)$ two excitation shapes with centre frequency $f = 700$ kHz are considered, namely: half cycle sine waveform, called case 'A' and one cycle sine waveform, called case 'B', which have been presented in Figure 3.

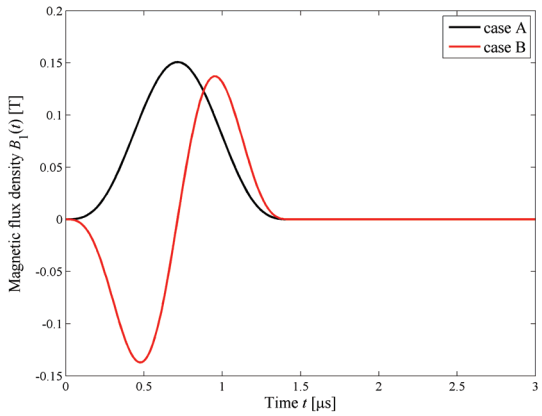

Fig. 3. Considered shapes of the pulsed magnetic field B_1: case A – half cycle sine waveform, case B – one cycle sine waveform

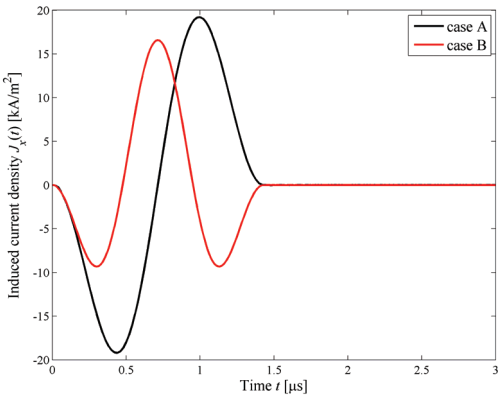

Fig. 4. Induced current density J_x component for case A and case B

The corresponding induced current density J_x components calculated at the interface between two layers for two shapes of pulsed magnetic field B_1 have been presented in Figure 4 (case A and case B).

Figure 5 shows the normalized acoustic waveform propagated circumferentially from the acoustic wave source (inner layer) at exemplary time t = 10 μs (case A).

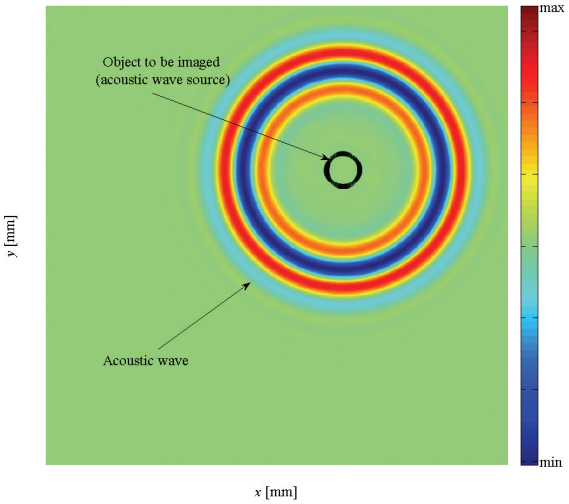

Fig. 5. Normalized acoustic waveform at exemplary time t = 10 μs (case A)

It is known that the acoustic pressure $p(\mathbf{r}, t)$ is proportional to the intensity of the vibration source. The vibration source corresponds to the Lorentz force divergence $\nabla\cdot(\mathbf{J} \times \mathbf{B}_0)$, as shown in equation (4). In order to reconstruct the vibration source position the time reversing technique has been applied. The reconstruction has been performed with the help of the Matlab k-Wave toolbox based on the finite difference time domain (FDTD) [10, 12].

The drawback with the classical finite difference approach using computational grid is the fact that the total number of degrees of freedom is too high to solve the problem using standard PC computer, especially when the problem is considered in 3D space. The k-Wave toolbox uses the *k*-space pseudospectral method (or called *k*-space method) and in such an approach one can achieve reducing the memory and number of time steps required for accurate simulations. Finally, in simulations two points per acoustic wavelength (instead of ten) are required. The assumption is based on the Fourier collocation method. The Fourier collocation spectral method is responsible for discretization in the spatial domain but to calculate the gradient in the time domain the finite difference schemes is used [12].

In calculations the measuring points as transducers' equivalents have been used. Utilizing the recorded pressure time signals, an image of the vibration source can be obtained. It is assumed that the studies are ideal and thereby, the recorded signals are noise-free. The measuring points have been placed on the circumference of the virtual circle. The circle has a constant diameter equal to 60 mm and is situated non-coaxially relative to the object to be imaged

(Fig. 2). Fig. 6 show the reconstruction results obtained for 24 measuring points (15° step), for case A (left) and case B (right), respectively.

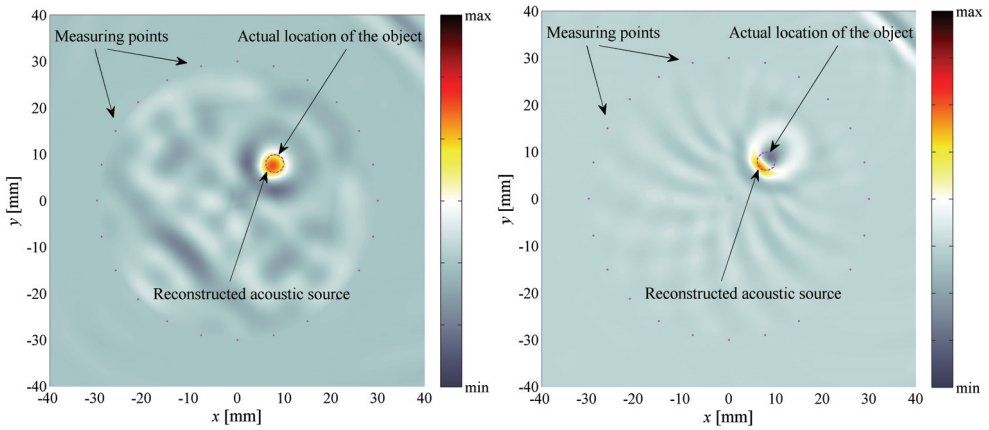

Fig. 6. Reconstruction of the acoustic source position for 24 measuring points, for case A (left) and case B (right)

It can be observed that in case A the reconstructed acoustic source position corresponds better to the actual location of the object of conductivity σ_1. Therefore, the case A (half cycle sine waveform of pulsed uniform magnetic field B_1) has been chosen to perform further calculations, i.e. image reconstruction of the two vibration sources of exemplary shapes with conductivity σ_1 = 10 S/m. In Figures 7-8 the reconstructed positions of the vibration sources for different number of measuring points equals to 12, 24, 36 and 72, have been presented respectively.

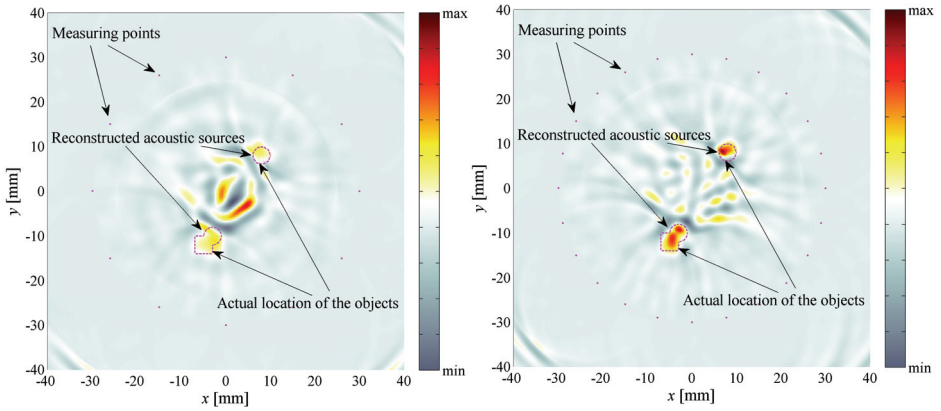

Fig. 7. Reconstruction of the acoustic source position for 12 (left) and 24 (right) measuring points

In the reconstructed images some blurring artifacts around and between the objects can be observed. The worst case is for 12 measuring points (Fig. 8), as expected. However, more measuring points leads to a better quality images with less time reversal noise. In case of 72

measuring points the reconstructed acoustic sources positions almost exactly correspond to the actual locations of the objects. In this case the overall contrast pattern is well reconstructed, with some small disturbances located at the objects' boundaries.

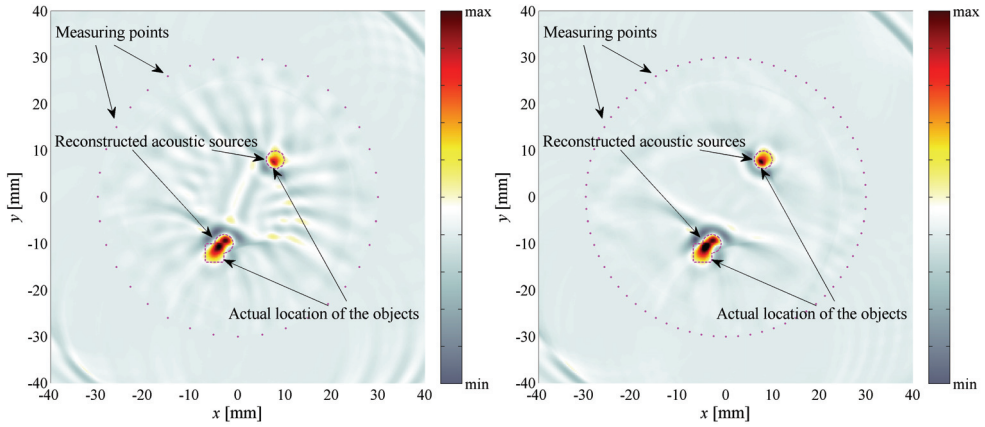

Fig. 8. Reconstruction of the acoustic source position for 36 (left) and 72 (right) measuring points

4. Conclusions

One of the advantageous features of MAT-MI technique is its good image contrast, high spatial resolution and absence of the shielding effect. The presented simulations of MAT-MI demonstrate the feasibility and performance of such a tomography to image objects which have conductivity values close to those of biological tissues. This property may have important applications to clinical diagnosis, such as early detection of small cancers or tumours.

In this paper the 2D MAT-MI forward and inverse problem simulations have been conducted. According to the inverse problem the acoustic vibration source (Lorentz force divergence) position has been identified, and for conductivity distribution reconstruction the governing equations have been provided. In order to image the conductivity distribution within the entire object a 3D finite element model is required.

References

[1] Haemmerich D., Staelin S.T., Tsai J.Z. et al., *In vivo electrical conductivity of hepatic tumours.* Physiological Measurement 24: 251-260 (2003).

[2] Fear E.C., Hagness C., Meaney P.M. et al., *Enhancing breast tumor detection with near-field imaging*. IEEE Microwave Magazine, March 2002, p. 48-56 (2002).

[3] Li X., Xu Y., He B., *Imaging electrical impedance from acoustic measurements by means of magnetoacoustic tomography with magnetic induction (MAT-MI)*. IEEE Transactions on Biomedical Engineering 54(2): 323-330 (2007).

[4] Cichon-Bankowska K., Ziolkowski M., Gratkowski S. et al., *Magnetoacoustic tomography with magnetic induction for low conductivity objects.* Acta Bio-Optica et Informatica Medica Inżynieria Biomedyczna 20(4): 187-192 (2014).

[5] Wang H., Liu G., Jiang L., Li S., *3D inverse problem of magnetoacoustic tomography with magnetic induction.* Proceedings of the 5th International Conference on Information Technology and Application in Biomedicine, in conjunction with The 2nd International & Summer School on biomedical and Health Engineering, Shenzhen, Chiny, 30-31th of May (2008)
[6] Xia R., Li X., He B., *Reconstruction of vectorial Acoustic Sources in Time-Domain Tomography*. IEEE Transactions on Biomedical Engineering 28(5): 669-675 (2009).
[7] Xu Y., He B., *Magnetoacoustic tomography with magnetic induction (MAT-MI).* Physics in Medicine and Biology 50: 5175-5187 (2005).
[8] Stawicki K., Gratkowski S., Komorowski M., Pietrusewicz T.: A new transducer for magnetic induction tomography. IEEE Transactions on Magnetics, vol. 45, 3/2009, p. 1832-1835.
[9] Ma Q., He B., *Magnetoacoustic tomography with magnetic induction: a rigorous theory.* IEEE Transactions on Biomedical Imaging 55(2): 813-816 (2008).
[10] Fink M., *Time reversal in acoustics.* Contemporary Physics 37(2) 95-109 (1996).
[11] http://www.zfm.ethz.ch/alumni/leutenegger/Time_Reverse.htm, accessed February (2015).
[12] http://www.k-wave.org, accessed February (2015).